Published online 18 November 2022

NAR Genomics and Bioinformatics, 2022, Vol. 4, No. 4 **1**
https://doi.org/10.1093/nargab/lqac085

Mapping separase-mediated cleavage in situ

Abdelhalim Boukaba, Qiongfang Wu, Jian Liu, Cheng Chen, Jierong Liang, Jingjing Li and Alexander V. Strunnikov*

Molecular Epigenetics Laboratory, Guangzhou Institutes of Biomedicine and Health, Guangzhou, Guangdong, 510530, China

Received May 26, 2022; Revised October 13, 2022; Editorial Decision October 24, 2022; Accepted October 25, 2022

ABSTRACT

Separase is a protease that performs critical functions in the maintenance of genetic homeostasis. Among them, the cleavage of the meiotic cohesin during meiosis is a key step in producing gametes in eukaryotes. However, the exact chromosomal localization of this proteolytic cleavage was not addressed due to the lack of experimental tools. To this end, we developed a method based on monoclonal antibodies capable of recognizing the predicted neo-epitopes produced by separase-mediated proteolysis in the RAD21 and REC8 cohesin subunits. To validate the epigenomic strategy of mapping cohesin proteolysis, anti-RAD21 neo-epitopes antibodies were used in ChIP-On-ChEPseq analysis of human cells undergoing mitotic anaphase. Second, a similar analysis applied for mapping of REC8 cleavage in germline cells in Macaque showed a correlation with a subset of alpha-satellites and other repeats, directly demonstrating that the site-specific mei-cohesin proteolysis hotspots are coincident but not identical with centromeres. The sequences for the corresponding immunoglobulin genes show a convergence of antibodies with close specificity. This approach could be potentially used to investigate cohesin ring opening events in other chromosomal locations, if applied to single cells.

INTRODUCTION

Separase, or separin, is a cysteine protease (1,2,3–5) that has multiple cellular functions, both signaling (6–9) and enzymatic. The latter includes chromosome segregation (6,10–14), centrosome cycle (15–19) and DNA repair (20–22). Separase was discovered initially as a regulator of mitotic spindle (23–25) and was later recognized as a proteolytic enzyme that cleaves the SCC1/RAD21 subunit of somatic cohesin at the specific sites leading to the unlocking of cohesin ring-like structure and the ensuing resolution of sister chromatid cohesion in a highly regulated fashion (6,10,26–30). Separase also cleaves itself (31), as well as some non-cohesin proteins (32–34), and also has distinct non-enzymatic regulatory functions (9,35–38).

The essential target of separase, the cohesin complexes, are remarkable multifunctional protein machines, as they serve both in organizing the chromosomal compartmentalization of gene expression in interphase and are essential for maintaining and releasing sister chromatid cohesion at specific times during mitotic and meiotic cycles (Figure 1A and B). In metazoans, similar to lower eukaryotes (10), the release of cohesion between sister chromatids in mitotic cell division (12) is as essential as the establishment of proper cohesion itself (39). While the somatic cohesin complex is removed from chromosomes in two well known complementary mechanisms, i.e. stripping of cohesin from chromosomal arms in mitotic prophase in preparation for condensation and the cleavage of RAD21 at anaphase (40), the unloading of meiotic cohesins is more complex. Not only there are more cohesin complexes present in germline, but both the temporal program and the regulation of their removal is substantially more multifaceted. Furthermore, revealing the details of meiotic cohesins removal in metazoa, e.g. mice, is challenging, as mei-cohesin mutants arrest before the proteolytic cleavage normally takes place. The functional compartmentalization of centromeric, pericentromeric and arm cohesion, which is demanded by two meiotic divisions, poses an additional impediment to research. It is generally accepted, mostly on the basis of mouse germline studies, that several cohesin complexes coexist in mammalian germline cells, with at least two of them characterized in greater detail: REC8 and RAD21L cohesin complexes (41). While RAD21L is not present in lower eukaryotes, REC8 appears to be the universal meiotic cohesin subunit, which plays a key role in meiotic segregation of both chromosomes and chromatids (42–47). This makes REC8 cleavage by separase in meiosis even more intriguing, especially the specific role of REC8 proteolysis and protection from it at centromeres. Indeed, during spermatogenesis, REC8 likely functions in the cohesion of centromeres (48), despite RAD21L also localizing to centromeres and peri-centromeres in meiosis I metaphase (44). In *C. elegans*, the REC8-based cohesin complex is resistant to stripping by WAPL and therefore is dependent on REC8 cleavage

*To whom correspondence should be addressed. Tel: +86 20 32093734; Fax: +86 20 32015283; Email: alexstrunnikov@gmail.com

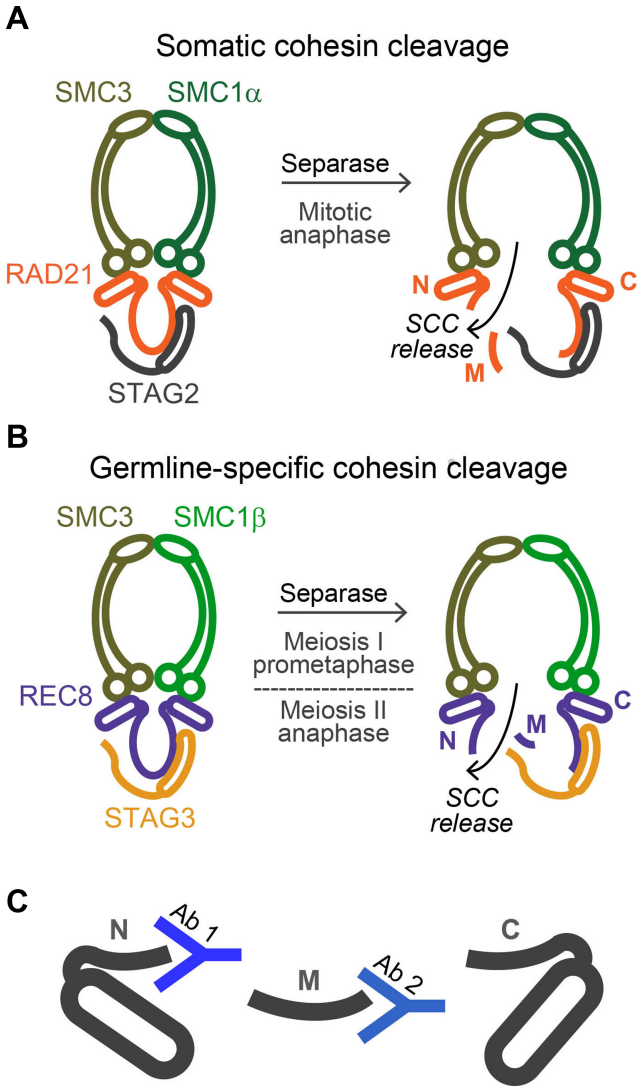

Figure 1. The principal design of the approach. (**A**) A schematic view of somatic (RAD21-based) cohesin complexes and the proteolysis at the metaphase to anaphase transition. The three proteolytic fragments are designated RAD21*N, RAD21*M and RAD21*C. (**B**) A depiction of germline-specific (REC8-based) cohesin complexes and the approximate times of proteolysis at the prometaphase of meiosis I, and anaphase of meiosis II. The three proteolytic fragments are designated REC8*N, REC8*M, and REC8*C. (**C**) The general strategy of desired antibody specificity to detect the neo-epitopes at the COOH-termini of *N and *M proteolytic fragments.

(49). Similarly, REC8 removal in human cells is also facilitated by separase, as the expression of non-cleavable mutant REC8 in mice causes the defects in chiasmata resolution, with males displaying sterility due to the production of spermatocytes with 4C DNA content, and oocytes manifesting a delay and disorganization of chromosome segregation in meiotic anaphase I (50).

In this work, we developed a promising approach to map separase cleavage events in situ, using meiotic cohesin targets as the source of antigens to develop cleavage-specific monoclonal antibodies (mAbs). The approach was validated using the RAD21 subunit of somatic cohesin and then applied to the REC8 subunit of mei-cohesin.

MATERIALS AND METHODS

Antibody production

mAbs were generated according to published protocols. Briefly, the epitope sequence was cloned into the VLP virus vector, the packaged virus particles were purified and concentrated. BALB/C mice were immunized with the corresponding VLPs and monitored for the immune response with ELISA of mouse serum. After 4 weeks, mouse spleen cells were fused with SP2/0 myeloma cells to make hybridomas. Positive clones were selected from ∼5000 clones in HAT medium in 96-well plates. Positive cell lines, after about five division cycles, were expanded and rescreened for clonal purity. The cultures were then passaged for 45 days to test for the stability of mAb production; and a fraction of the population was transplanted into the abdominal cavity of mice for 2 weeks to induce ascites, while the rest of the culture was frozen. Ascites fluids were removed and the antibodies were purified with ProteinA/G resin. In order to eliminate any possibility that the Abs might recognize the uncleaved REC8 or RAD21, they were counter-purified against oligopeptides corresponding to the uncut proteins, and then affinity purified with the resin coupled to the cleavage-mimicking peptides.

Antibody selection and testing

To select ChIP-seq grade mAbs, the ascites were screened using several approaches. First, the GST fusions with the sequences encoding peptides corresponding to cleavage-site epitopes, as well as peptides with both shorter and longer sequences (Supplementary material) were expressed in *E. coli* and probed by immunoblotting. Second, the full-length cDNA fragments corresponding to REC8, REC8*N, REC8*NM, REC8*M, RAD21, RAD21*N, RAD21*NM and RAD21*M were expressed in human HEK293 cells and also probed by immunoblotting as well as immuno-precipitations, in both cases mimicking the ChIP conditions, as recommended by Encode.

Hybridoma Ig genes sequencing

Total RNA was isolated from hybridoma cells using the RNA-easy Isolation Reagent (Vazyme) and reverse transcribed using isotype-specific anti-sense primers (proprietary of GenScript) or universal primers using SMARTScribe Reverse Transcriptase (Takara). The fragments of VH and VL were amplified according to the standard rapid amplification of cDNA ends (RACE) (GenScript). The amplified fragments were cloned into a PCR-cloning vector and DNA sequences were aligned to generate the consensus sequence for each hybridoma.

Cell culture, transfection and FACS

The DLD-1 (ATCC® CCL-221™) cell line was cultured in IMDM (Hyclone) with 10% FBS, HEK293 (ATCC® CRL-1573™) cells—in DMEM/10% FBS (Hyclone), and MOLT-4 (www.proteinatlas.org/ENSG00000100918-REC8/cell) were grown in RPMI-1640 /10% FBS. Plasmid transfections were as suggested by Roche for the X-tremeGENE 9 DNA transfection reagent.

To synchronize DLD-1 cells, 2×10^6 to 3×10^6 cells were plated into a 10 cm culture dish at 20–30% confluence and incubated overnight. Then, thymidine, 2 mM final concentration, was added, and the culture was incubated for 18 h. After washing cells with 10 ml of pre-warmed 1x PBS, pre-warmed fresh medium was added, followed by a 12 h incubation, then 2 mM thymidine was added the second time, followed by 24 h incubation. G1/S cells were then released into pre-warmed fresh media after washing with 1× PBS. Samples were collected for immunoblotting and FACS at 0 h to 13 h time points.

For FACS analysis, trypsin was applied to cells for 3 min; cells were harvested, washed 3 times with DPBS, spun down and resuspended in 0.3 ml of DPBS. Cells were fixed by adding 0.75 ml of ice-cold ethanol, drop by drop with vortexing, followed by the incubation at 4˚C. To stain cells, 200–400 μl of propidium iodide and RNase staining buffer (BD Pharmingen) was added, with gentle mixing, for 15 min at 37˚C. Flow cytometry was done using BD LSR Fortessa SORP Flow Cytometer, with 25 000 events recorded per sample.

Testis immunohistochemistry

Anti-REC8* mAbs were tested in the immuno-chemical staining of thin paraformaldehyde fixed and paraffin embedded (PFPE) sections of human testis (Alenabio Biotechnology Co., Xian, China). IHC was carried out using standard protocols for paraffin-embedded tissues, with antigen recovery by boiling in 10 mM sodium citrate buffer in a microwave oven.

Human cells immunofluorescent staining

The mAbs against RAD21* neo-epitopes were screened by staining DLD-1 cells cultured on glass coverslips. They were washed 2 times with PBS, fixed with 4% paraformaldehyde/PBS for 15 min, and the fixation was quenched and cell permeabilized simultaneously in TBS-T (100 mM Tris pH 8.0, 20 mM glycine, 1% Triton X-100, 0.05% Tween-20) 2 times × 10 min. The primary mAbs corresponding to RAD21* neo-epitopes and anti-CREST (15-234-0001, Antibodies Inc.) were added in TBS-T with 10% horse serum or BSA. After the incubation for 1 h at 23°C or overnight at 4°C, coverslips were washed 3 times for 5 min with TBS-T, and the secondary Abs mixed with DAPI were added in TBS-T with 10% horse serum or BSA for 1 h at 23°C. Cells were washed 3 times for 5 min with TBS-T, and mounted onto microscopy slides in mounting media (ab104135). The microphotographs were captured with confocal Zeiss microscopes LSM710 and LSM800 or Leica SP8 Lightning. The 3D image deconvolution was performed with Huygens Software (Scientific Volume Imaging B.V.).

Chromatin fractionation

Fractionation of chromatin from cultured cells was as in (51). About 10^7 cells were washed in PBS at 4°C, resuspended in 200 μl per sample of buffer A (10 mM HEPES pH 7.9, 1.5 mM $MgCl_2$, 10 mM KCl, 1 mM DTT, 0.34 mM sucrose, 10% glycerol, Roche protease inhibitor cocktail). Triton-X100 was added to 0.1% final concentration, samples were kept on ice for 10 min, and spun at 1300 × g for 5 min at 4°C. The supernatant (S1) was additionally centrifuged for 5 min at 20 000 × g, 4˚C, producing the S2 fraction. The crude nuclei pellet was washed once with buffer A, resuspended in 100 μl of buffer B (3 mM EDTA, 0.2 mM EGTA, 1 mM DTT, Roche PIC), and nuclei were lysed for 30 min on ice. The lysate was centrifuged at 1700 × g for 5 min at 4˚C, and the supernatant (S3) was stored on ice. The chromatin-enriched pellet, i.e. fraction P3, was washed in buffer B, and then resuspended in 100 μl of SDS loading buffer.

Cloning and PCR

Sequences encoding cleavage site peptides and control peptides were derived by annealing the corresponding oligonucleotides, followed by cloning into the BamHI and EcoRI sites of pGEX-6p-1 vector. For mammalian expression vectors, PCR sequences were cloned into pCMV6-Entry plasmids at the AsiSI/MluI sites and 3xMyc tags were added at the N-terminus of each ORF at the AsiSI site. PCR was done with KOD-401 polymerase (Toyobo) in a 2720 thermocycler (Applied Biosystems).

ChIP-on-ChEPseq analysis

The off-site (Wincon TheraCells Biotech., Nanning, Guangxi, PRC) animal care was in compliance with the ethical standards and national/international guidelines (52,53), and has been approved by the institutional review board. Cynomolgus macaques' (*Macaca fascicularis*, *M. fasc.*) testis material was from males that were 7 to 9 years old, which were sacrificed for an unrelated study, after the animal protocol was amended to include post mortem testis removal, as per Good Laboratory Practices and the WHO guidelines.

Testes were processed on site for germ cells preparation. Samples were fragmented into pieces with sterile scalpel while on ice and the resulting homogenates were filtered through 100-μm mesh wire gauze, thus removing larger tissue fragments. Cells were washed 3 times with cold PBS, followed by the 15 min fixation with 1% formaldehyde in PBS. The reaction was quenched with 0.125 M glycine (final concentration); the cells were centrifuged at 200 × g, resuspended in PBS with 10% glycerol and 1× cocktail of Roche proteinase inhibitors, and stored at −80˚C. Before use, samples were thawed on ice and passed through a 40 μm cell strainer with cold PBS.

For ChIP-On-ChEPseq, a published procedure named ChEP (Chromatin Enriched for Proteomics) was adapted to extract pure fixed chromatin under stringent chaotropic conditions (54). 10 to 20 million germ cells were resuspended in 1 ml of nuclei lysis buffer (25 mM Tris–HCl, 85 mM KCl, 0.1% Triton-X100, pH 7.4, Roche PIC), centrifuged at 2300 × g, resuspended again in the same buffer containing 200 μg/ml RNase A, and the samples were incubated in thermomixer at 37˚C for 15 min at 1000 rpm. After that, samples were spun at 2300 × g for 5 min at 4˚C, pellets were resuspended in 500 μl (per 10^7–2×10^7 nuclei) of nuclei disrupting buffer (4% SDS, 50 mM Tris–HCl, 10 mM

EDTA, pH 7.4), and mixed with 1.5 ml of urea buffer (8 M urea, 10 mM Tris–HCl, 1 mM EDTA, pH 7.4). After gentle mixing leading to the clarification of the solution, it was centrifuged at 16 100 × g for 30 min at 23°C. After decanting of the supernatant, resulting pure chromatin was washed twice with ChIP sonication buffer (20 mM Tris–HCl, 150 mM NaCl, 1% Triton-X100, 0.1% Na deoxycholate, 0.1% SDS, 1 mM EDTA, 1 mM PMSF), and samples were reconstituted with sonication buffer to 1 ml volume. Chromatin fragmentation was done in 2-ml tubes in Covaris S220 with the following settings: 100 W peak incident power, 10% duty factor, 10 W average incident power, 30/30 s duration/delay, 200 cycles/burst, 30 repeats. A similar chromatin preparation protocol was also used for DLD-1 cell culture.

For the immunoprecipitation, fragmented chromatin aliquots (∼100–150 μg per 1 ml of ChIP buffer) were thawed on ice, and 10 μg of specific Ab was added. Magnetic beads with no specific antibodies bound or proteinA/G magnetic beads were used as a negative control. Anti-human SMC3 Ab (ab9263) was used as a general cohesin-recognizing reference, for both somatic and meiotic cohesins, and anti-CENP-A (ab13939) for centromere pull down. First, samples were incubated with a primary Ab at 4°C overnight with end-to-end rotation. Then, 120 μl of sheep anti-rabbit or anti-mouse IgG magnetic beads (ThermoFisher), prewashed with 3 × 1 ml ChIP buffer, were added. Samples were incubated about 4 h at 4°C, with mixing, and then separated with a magnetic stand (ThermoFisher). The beads were washed sequentially: 2× with 1 ml ChIP buffer, 4°C for 5 min each, 2x with 1ml of ChIP high salt buffer (20 mM Tris–HCl, 500 mM NaCl, 1% Triton-X100, 0.1% Na-deoxycholate, 0.1% SDS, 1 mM EDTA), 2× with 1 ml of LiCl buffer (20 mM Tris–HCl, 1% NP-40, 0.5% Na-deoxycholate, 0.25 M LiCl, 1 mM EDTA, 0.1% SDS, pH 8), and 2× with 1 ml of TE buffer. To release the captured chromatin fragments, beads were resuspended in 200 μl of elution buffer (TE with 1.5% SDS) and incubated on a Thermomixer (Eppendorf) at 65°C, 30 min, 1000 rpm. Beads were then re-extracted again, as above, the eluates were pooled together and incubated overnight at 65°C. Proteinase K (ThermoFisher) was then added for 1 h at 50°C, and DNA extraction was done using PCR purification kit (Qiagen) in ∼70 μl buffer (0.1× TE, pH 8). 5μl of DNA solution was used for the quantification by Qubit (ThermoFisher). The precipitated DNA were processed and sequenced at WuXi App (Shanghai).

Bioinformatic analysis

The NGS' paired reads were initially cleaned from low quality reads and adapters using fastp (55). For genome-wide analysis, tags were aligned using Bowtie (56) to the human genome GRCh38.p12 (hg38), NCBI Assembly ID: 5800238, or crab-eating macaque (female) genome assembly Macaca_fascicularis_5.0 (Macfas5, NCBI Assembly ID: 704988). Bowtie parameters were: -best -m 5 -v 3 (for 150 nt reads). Peak calling with MACS2.2 (57,58) was limited to chromosome-assigned elements, with input ChIP-seq reads used as a reference. Additional peak filtering steps: first, the summits of high confidence (based on q-value) peaks were intersected with RepeatMasker (RM) and Tandem Repeat Finder (TRF) datasets, and then the peaks with summits in repeats were excluded; second, peaks from two biological replicates were intersected with each other with bedtools (59), using –d 10 parameter, or with Genome Integrator (UCSC utilities), to generate a set of conserved peaks; third, noisy intervals were removed after tag density clustering at peaks' summits using DeepTools (60) or Seqminer (61).

Analysis of repeated DNA enrichment was done separately from genome-wide analysis. Tag density files were generated and concatenated for two animals or for two independent replicates in case of human cells. Alignments were done using bowtie2 with –bowtie2-sensisitvity-level very_sensitive parameter. Sequencing reads from human cells were aligned to the catalogued human centromeric repeats from (62), which were tandemly duplicated to generate a contiguous repeat junction, and hit counts were normalized relatively to the total number of clean reads for each sample. As no bona fide centromere-resident repeats were previously validated in *M. fascicularis,* first all the repeats present in the current assembly were extracted by Tandem Repeat Finder (tandem.bu.edu/trf/trf) (63,64). Only *M. fascicularis* repeats that were at least 120 bp long were selected for subsequent analyses. They were also duplicated in tandem and used for sequencing tags alignment.

RESULTS AND DISCUSSION

Generation and validation of monoclonal antibodies against RAD21 proteolytic neo-epitopes

To address the epigenomic topography of REC8 cleavage in meiosis, first, one needs a reagent that could distinguish a full-length cohesin subunit REC8 from a proteolytically cleaved fragment generated by separase (Figure 1B). That could be feasible, via the generation of antibodies specifically directed against the neo-epitopes produced by the separase-mediated proteolysis (Figure 1C). Prior to approaching the actual task of analyzing REC8 cleavage in meiosis we tested the feasibility of the proposed method by assessing the cleavage of the somatic RAD21 (Figure 1A), because it is feasible to generate a synchronous population of anaphase cells in culture and because the chromosomal location of cleavable RAD21 pool is known for metaphase-to-anaphase transition. The task was to make such a specific antibody that is able to recognize the COOH-termini resulting from RAD21 proteolysis by separase *in vivo* (Figure 2A). As previous studies have provided sufficient information on the specificity of cleavage sites in mammalian RAD21/SCC1 (65), we focused on two major cleavage sites identified in (66). While the RAD21*M product of separase-mediated cleavage is prone to degradation in every cell cycle (65), the relative kinetic of the cleavage of two sites in vivo is not known. Therefore, we assessed both the RAD21*N and RAD21L*M fragments as COOH- neo-epitope antigens (Figure 2A).

To obtain mouse monoclonal antibodies with such a specificity, the polypeptides that mimic the RAD21 cleavage sites, DREIMR and IEEPSR (Figure 2A), were used for mice immunization. For the screening, we also used negative

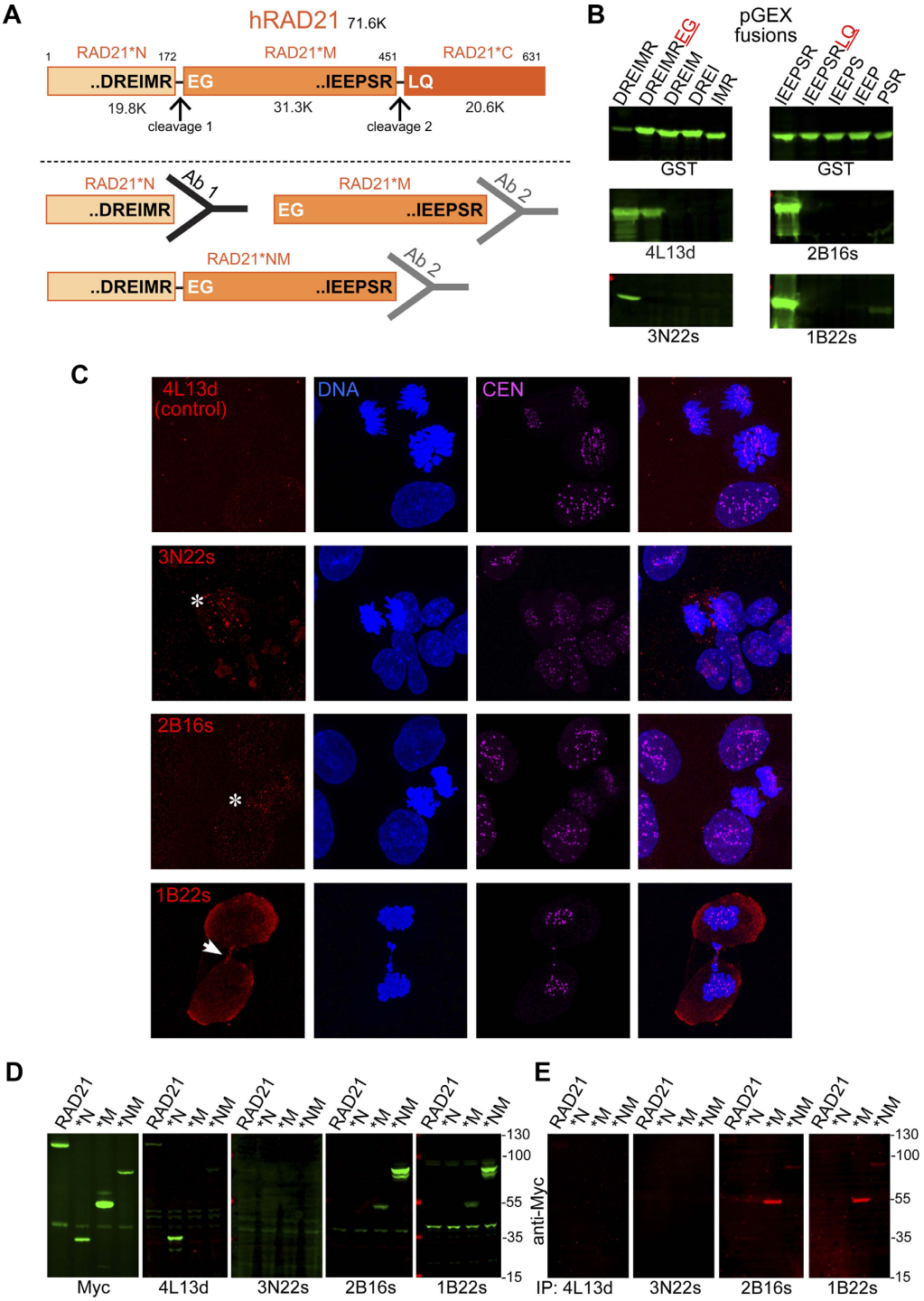

Figure 2. Characterization of monoclonal antibodies against RAD21* neo-epitopes. (**A**) The positions of two cleavage sites inferred from the mouse RAD21. The positions of amino acid residues are above, and the predicted molecular weights are shown below for the three fragments. Lower panel displays the projected specificity of Abs; Ab specific for the site 2 is also expected to recognize the N + M fragment. (**B**) Immunoblotting of E. coli extracts expressing peptides corresponding to the vicinity of cleavage sites in human RAD21 fused to GST. The antibodies 4L13d is a control mAb that should recognize an uncleaved site 1 of RAD21, 3N22s was against the DREIMR peptide (site 1), while 1B22s and 2B16s were against IEEPSR (site 2). The antibodies, except, predictably, 4L13d, have high specificity against the fusion proteins mimicking the corresponding cleaved RAD21 residues. (**C**) Immunofluorescent staining of DLD-1 cells with anti-RAD21* mAbs. CREST staining shows centromeres. The asterisks denote mitosis-specific RAD21* mAbs staining. The arrow indicates the sub-spindle staining in late anaphase. (**D**) Immunoblotting with mAbs against extracts of HEK-293 cells that express the predicted products of RAD21 cleavage. This testing was a part of assessing mAbs for satisfying ChIP-grade criteria. The whole cell extracts derived from transient transfection of plasmid expressing RAD21* fragments were probed with the corresponding mAbs. The immunoblotting was done in RIPA buffer mimicking ChIP conditions. The 3N22s mAb failed in this test. (**E**) Immunoprecipitations with mAbs to RAD21* neo-epitope under ChIP conditions. Extracts from transfected HEK-293 cells, as in (D), were prepared for ChIP and processed according to the standard Encode protocol. The 2B16s and 1B22s mAbs have passed the test, while 3N22s failed. IP, immunoprecipitating mAb.

control peptides, which had two extra residues at the COOH terminus of the corresponding cleavage site: DREIMREG and IEEPSRLQ, respectively. Ascites samples from selected hybridomas (see Methods) were used in immunoblotting to screen the GST-fused peptides with the COOH-termini matching the RAD21* termini, as well as a number of both shorter and longer fusions as controls. As a result, we identified clones with various degrees of desired specificity for RAD21*N and RAD21*M termini (Figure 2B). The control mAb, 4L13d, which corresponded to an uncleaved site 1, did recognize both DREIMR and DREIMREG fusions, but not the C-terminally truncated fusions (Figure 2B). Curiously, the absence of the glutamate residue at the –4 position from the cleavage site either abolished or severely diminished antibody binding in all cases, likely indicating that, these mAbs were directed not just against the three COOH-terminal residues.

These four mAbs were first tested for their ability to work in immunofluorescent (IF) staining of human cells in culture (Figure 2C). The 4L13d mAb, i.e. uncleaved RAD21 control, did not show any mitosis-specific staining. The 3N22s, 2B16s and 1B22s displayed some distinct mitosis-specific staining of speckles only partially associated with chromosomes. In addition, the 3N22s mAb also stained some chromatin territories in interphase cells (Figure 2C). While the 1B22s mAb had higher background overall, it gave specific staining in anaphase cells corresponding to spindle mid-zone (Figure 2C). The observed IF signal, however, should be interpreted cautiously, as it cannot be unambiguously attributed to RAD21 alone. For example, separase itself also contains an EIMR* self-cleavage site (31) and was shown to localize to a number of subcellular locations in non-human systems (35,37,38), while in human cells it is predominately cytoplasmic in interphase and centrosomal in mitosis (67,68). The latter might explain the staining of non-chromosomal foci in Figure 2C.

Next, the mAbs were tested against recombinant RAD21 protein fragments, which mimicked the predicted cleavage products, expressed ectopically in a human cell line. First, immunoblotting was conducted with both mAb binding and washing under standard ChIP buffer conditions (69). As expected, the 4L13d mAb recognized both full length RAD21 and the RAD21*N fragment (Figure 2D). One anti-RAD21*N antibody, 3N22s has failed this validation step, indicating that this mAb cannot be deemed a ChIP-grade one, while the 2B16s and 1B22s mAbs have passed this test (Figure 2D). We also analyzed the four mAbs using IP recapitulating a ChIP protocol in human cells, except that chromatin crosslinking was omitted. As shown in Figure 2E, only anti-RAD21*M-specific mAbs were able to pull down the corresponding polypeptides. Thus, we generated and characterized two independent ChIP-grade mAbs against a COOH-terminal neo-epitope resulting from RAD21 cleavage by separase.

Generation and validation of monoclonal antibodies against REC8 proteolytic neo-epitopes

Mapping of mammalian REC8 cleavage sites was previously done only in mice, revealing three of multiple EXXR sites as bona fide proteolysis sites in vitro and vivo (50), just two of which are conserved in human REC8 protein. As in the case of RAD21 above, we chose both REC8*N and REC8*M fragments, even though they incidentally terminate with two identical residues (Figure 3A).

In order to generate a pool of monoclonal antibodies, mice were immunized with specific polypeptides LLEIPR or EIEVPR. Upon obtaining a high titer of polyclonal antibodies that reacted specifically with these two peptides, but not with control C-terminally extended peptides, hybridomas were generated and subjected to ascites fluid analysis by immunoblotting. Screening the GST-fused peptides revealed a range of specificities, including the ones that appeared to be specific for REC8*N and REC8*M (Figure 3B). The absence of the –4 glutamate residue resulted in a reduction but not abolished mAb binding, suggesting that this residue is still partially recognized or affects the COOH-terminus structure (Figure 3B).

The immunohistochemistry (IHC) staining of thin sections of human testis with the three mAbs showed both cytoplasmic and nuclear staining in spermatocytes, which varied dependent of the stage of spermatogenesis (Figure 3C). Incidentally, only mAb 1E22d displayed a clear overlap of staining with chromosomes.

In the next step, the mAbs were validated for ChIP applications. First, we conducted immunoblotting with antibody binding under standard ChIP buffer conditions (Encode) using human cell extracts with ectopically expressed REC8, REC8*NM, REC8*N and REC8* M fragments (Figure 3D). The mAb against REC8*N COOH-terminus (2M17s) was also able to recognize the COOH-terminus of REC8*M, and vice versa (1E22d, Figure 3D). This implies that the native REC8*N and REC8*M are also unlikely to be distinguished by these mAbs in mammalian cells and extracts, which, however, does not diminish their utility.

In order to additionally interrogate mAbs with respect to REC8 expressed endogenously, we employed the MOLT-4 acute lymphoblastic leukemia cell line, where the *REC8* gene is activated and the corresponding protein is expressed, according to proteinatlas.org. Immunoblotting of MOLT-4 cell extracts after bulk chromatin fractionation indicated that REC8 protein is indeed produced in this cell line, albeit is not stably bound to chromatin without other meiocohesin partners (Figure 3E), as expected based on our recent work (70). All three monoclonal anti-REC8* antibodies detected two bands likely corresponding to REC8*N and/or REC8*M fragments, which were problematic to straightforwardly identify by immunoblotting, considering that MOLT-4 cells express several REC8 isoforms, based on proteomic data. Nevertheless, it is likely that these bands stained by both anti-REC8 and anti-REC8* antibodies resulted from the promiscuous activity of separase.

In the next step, we again tested the mAbs with ectopically expressed substrates by IP carried out under ChIP protocol conditions, without chromatin crosslinking. As shown in Figure 3F, the antibodies were efficient in immunoprecipitating the corresponding recombinant fragments. Thus, the 2M17s, 4M8s, and 1E22d mAbs recognizing the COOH-terminal neo-epitopes generated upon REC8 cleavage by separase were positively validated as ChIP-grade in this test.

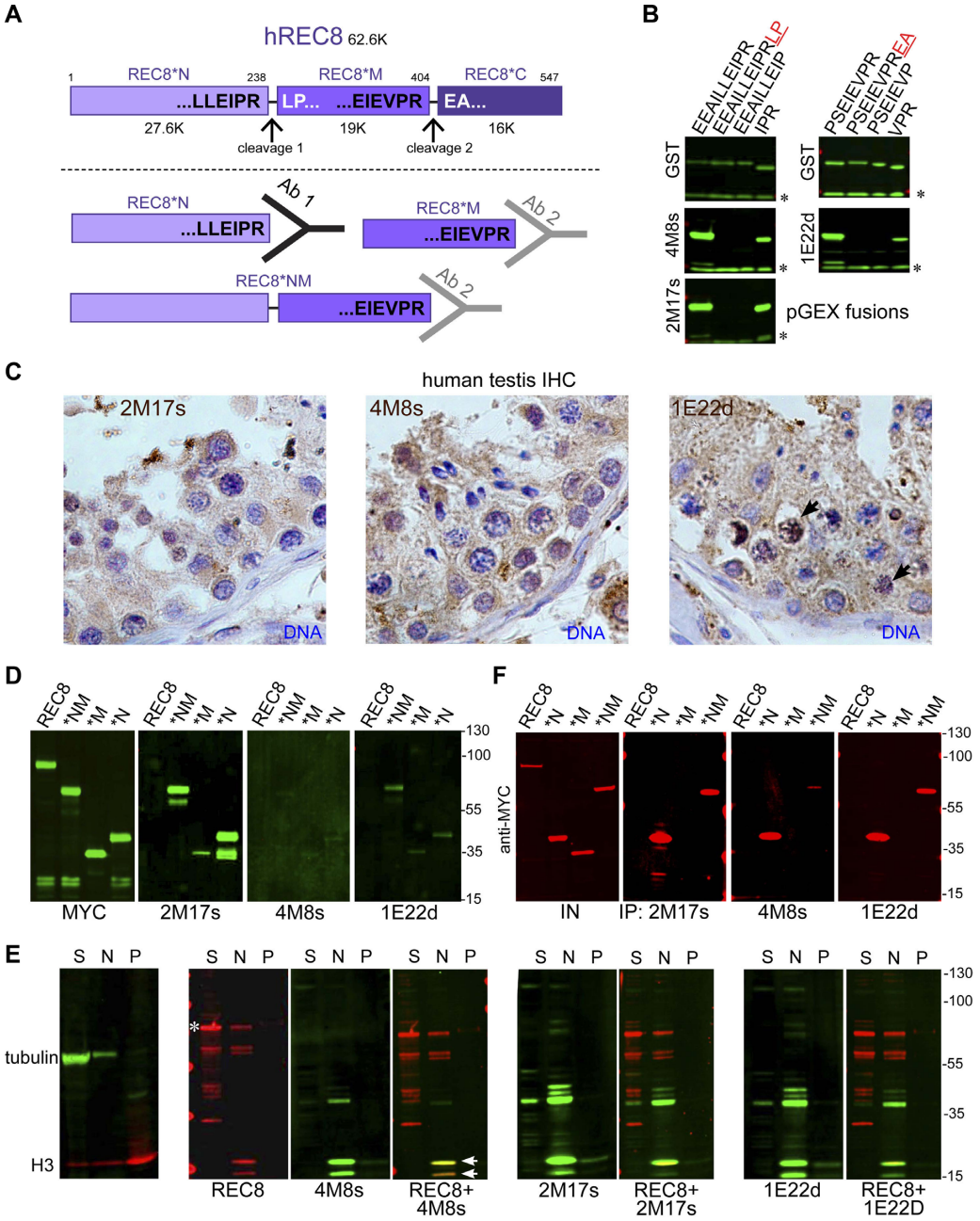

Figure 3. Characterization of monoclonal antibodies against REC8* neo-epitopes. (**A**) The locations of two cleavage sites inferred from the mouse REC8. The positions of amino acid residues are shown above, and the predicted molecular weights are below. Lower panel outlines the expected outcome of the designed Abs specific for the COOH-terminal neo-epitopes of REC8*N and REC8*M. (**B**) Immunoblotting of *E. coli* extracts expressing peptides corresponding to the vicinity of cleavage sites in human REC8 fused to GST C-terminally. The antibodies 2M17s and 4M8s were against EEAILLEIPR (site 1), and 1E22d mAb was against PSEIEVPR (site 2). The inclusion of several control peptides enables the demonstration that the mAbs recognize the specific residues corresponding to the cleaved REC8, and only when they are positioned C-terminally. Asterisk marks the position of background band. (**C**) Human testis IHC staining with anti-REC8* mAbs. Thin sections of human testis were stained with the three mAbs and counter stained with hematoxylin. The overlap of 1E22d staining with chromosomes is indicated with arrowheads. (**D**) Testing mAbs against extracts of HEK-293 cell line that expresses ectopic fragments of the expected products of REC8 cleavage. The whole cell extracts derived from transient transfection of plasmid expressing REC8* fragments, as indicated, were probed with the two mAbs originally derived from the immunizations against the site 1 epitope and one – against the site 2. The immunoblotting was done in RIPA buffer to test whether mAbs could recognize their epitopes under ChIP conditions. The three antibodies do not recognize the uncleaved REC8, but react with both site 1 and site 2 neo-epitopes, albeit with widely ranging avidity for both sites. (**E**) Testing mAbs against extracts of MOLT-4 cancer cell line that expresses endogenous REC8. This cell line expresses multiple REC8 isoforms, hence accurate prediction of the size of cleavage products is not feasible. REC8 antibodies immunoblotting shows that the bulk of the protein is not bound to chromatin pellet (P) but is distributed between the soluble (S) and nuclear unbound (N) fractions (indicated by asterisk). The anti-REC8* mAb detects two major bands (indicated by arrows), likely representing REC8 cleaved by separase. The fact that all three mAbs recognize the same bands suggests that they represent human REC8* COOH-terminal epitopes in vivo. Alpha-tubulin and histone H3 are fractionation markers. (**F**) Test IP with REC8* neo-epitope mAbs under ChIP conditions. Extracts from HEK-293, as in (C), were prepared for ChIP and processed according to the standard Encode protocol. All three mAbs: 2M17s, 4M8s and 1E22d were able to precipitate both REC8*N and REC8*N + M fragments. IN, input; IP, immunoprecipitate.

Epigenomic validation of mAbs against RAD21 proteolytic neo-epitopes

As human somatic cohesin subunit RAD21 is cleaved in a relatively narrow time window in anaphase (12), we used a synchronous cell population to validate our mAbs in ChIP-on-ChEPseq for mapping the specific mitotic proteolysis of somatic cohesin. DLD-1 cells were synchronized using a double thymidine block, with cells samples collected and analyzed by FACS and ChIP every 30 min after the release, beginning with the G2 phase. The transition from metaphase to anaphase was evident to occur between 8.5 and 9.5 h (Figure 4A).

The mAbs against the 2nd RAD21 cleavage site (RAD21*M), 1B22s and 2B16s, were employed in ChIP-on-ChEPseq experiments to locate the cleaved RAD21 still bound to chromatin. In order to diminish a chance of precipitating unrelated/cross-reacting proteins, analysis was focused only on sites that were bound by cohesin, as was determined by SMC3 pull-down conducted in parallel. First, we assessed the binding in the non-repeated part of human genome, by excluding all peaks with summits in the repeated DNA. As RAD21 cohesin complex is removed from chromosomal arms by a prophase pathway not involving cleavage by separase (12), we did not expect to find strong RAD21* peaks along the arms. Indeed, as shown in Figure 4B, the corresponding RAD21* neo-epitope tag density was at near background level for both stronger and weaker cohesin sites (Figure 4B and C).

Next, we turned to analyzing centromere repeats, where RAD21 cleavage should indeed occur at the metaphase to anaphase transition. From this analysis of 105,120 centromeric repeats (62,71), 105 027 sequences had at least one hit in one of the experiments. Initially, we focused only on a subset of repeats that had at least 500 hits before normalization in order to select robustly bound elements. That set was surprisingly small, with only 40 sequences, including 13 ALR repeats. As shown in Figure 4D, for the most enriched alpha satellites, the peak of enrichment coincided with early anaphase (from 8 to 10 hrs), suggesting that the mAbs likely recognized the proteolyzed RAD21 *in situ*. Alternatively, we filtered ALRs based on both enrichment ratio and tag density criteria. Based on these thresholds, the significantly enriched group (tag density $\geq$ 0.1 and fold enrichment $\geq$ 2) included 269 repeats common for 8 and 9 h time points (Figure 4E).

We also conducted a comparison of RAD21* enrichment at ALR with human CENP-A ChIP-seq data (72). Among 2097 ALRs enriched for CENP-A, RAD21* at 8 h, or RAD21* at 9 h (as described in Figure 4F), only 18 were enriched $\geq$2 for all three cases. 269 ALR repeats maximally RAD21*-enriched at 8 and 9 h, were used to derive a consensus ALR. This consensus notably deviated from HOR-forming ALRs, particularly within the CENP-B box (Figure 4G), which is consistent with a recent report on cohesin forming distinct subdomains within human centromeres and in pericentromeric regions (73). Alignment of RAD21*-enriched repeats to the full T2T human genome (74,75) showed that their numbers varied significantly from chromosome to chromosome and they were not found on chromosome Y.

Epigenome analysis of primate testis using mAbs against REC8 proteolytic neo-epitopes

In order to circumvent the infeasibility of obtaining a synchronous population of human spermatocytes undergoing REC8 cleavage we used testis from *M. fascicularis* and limited our analysis to repeated, particularly putative centromeric DNA. The rationale for the latter was that the cumulative antibody binding to repeated DNA, even in an asynchronous population of germ cells, would provide sufficient signal amplification, especially if an internal control is available. This approach is feasible, as the arrangement of putative separase cleavage sites in macaque REC8 protein is identical to human REC8 (Figure 5A), and thus they should be readily recognized by our antibodies upon cleavage.

First, we set out to identify the putative centromeric core elements in chromosomes of *M. fasc.*, by performing ChIP-On-ChEPseq using anti-CENP-A antibodies. Chromosomal binding of CENP-A has not been previously analyzed in primate meiosis, even though CENP-A is the core (76) and the most stable (77) component of mammalian centromeres. The quantification of binding for core centromere proteins by conventional ChIP-seq is also technically challenging (78), thus making the application of the denaturing protocol such as ChIP-on-ChEPseq highly warranted (70). CENP-A sequence tags were aligned to the full set of TR derived from raw genomic data (See Methods), including both ALRs and other TRs no shorter than 120 nt. For REC8* experiments, similarly to RAD21* case above, we used SMC3 binding as a reference. Cluster analysis of SMC3 enriched repeats (Figure 5B) indicated that among 1,802 repeats the clusters #1 and #3 were predominately bound by CENP-A, while the #2 cluster, which showed stronger REC8* signal, was represented by two forms of AluY SINE repeats. The comparison of enrichment of individual repeat species for CENP-A and REC8* (Figure 5C and D) indicated that REC8* signal was only meaningful for a small subset of alpha-satellites. The absence of canonical CENP-B boxes (78), which are needed for centromere nucleation (79), in the top-scoring REC8* ALRs might signify that the mei-cohesin predominately binds in the regions excluded from kinetochores.

Upon additional filtering for repeats that have concomitant enrichment for SMC3 and REC8* it is apparent that binding to AluY and simple repeats is prominent (Figure 5D). It is also evident that telomeric repeats and the centromeric satellite III are at the top of the enriched simple repeats list (80,81) (Figure 5D).

Immunoglobulin genes sequences for antibodies against cleavage site neo-epitopes

In order to obtain the representative protein sequence information for anti-RAD21* and REC8* neo-epitope mAbs, mRNA sequence was determined for mouse immunoglobulin genes of the corresponding hybridomas (See Materials and Methods). Mature Immunoglobulin molecules are formed by joining heavy and light chains, both of which carry variable regions, VH and VL, respectively (Supplementary Figure S1A). Antigen binding specificity itself is mostly determined by the complementarity-determining re-

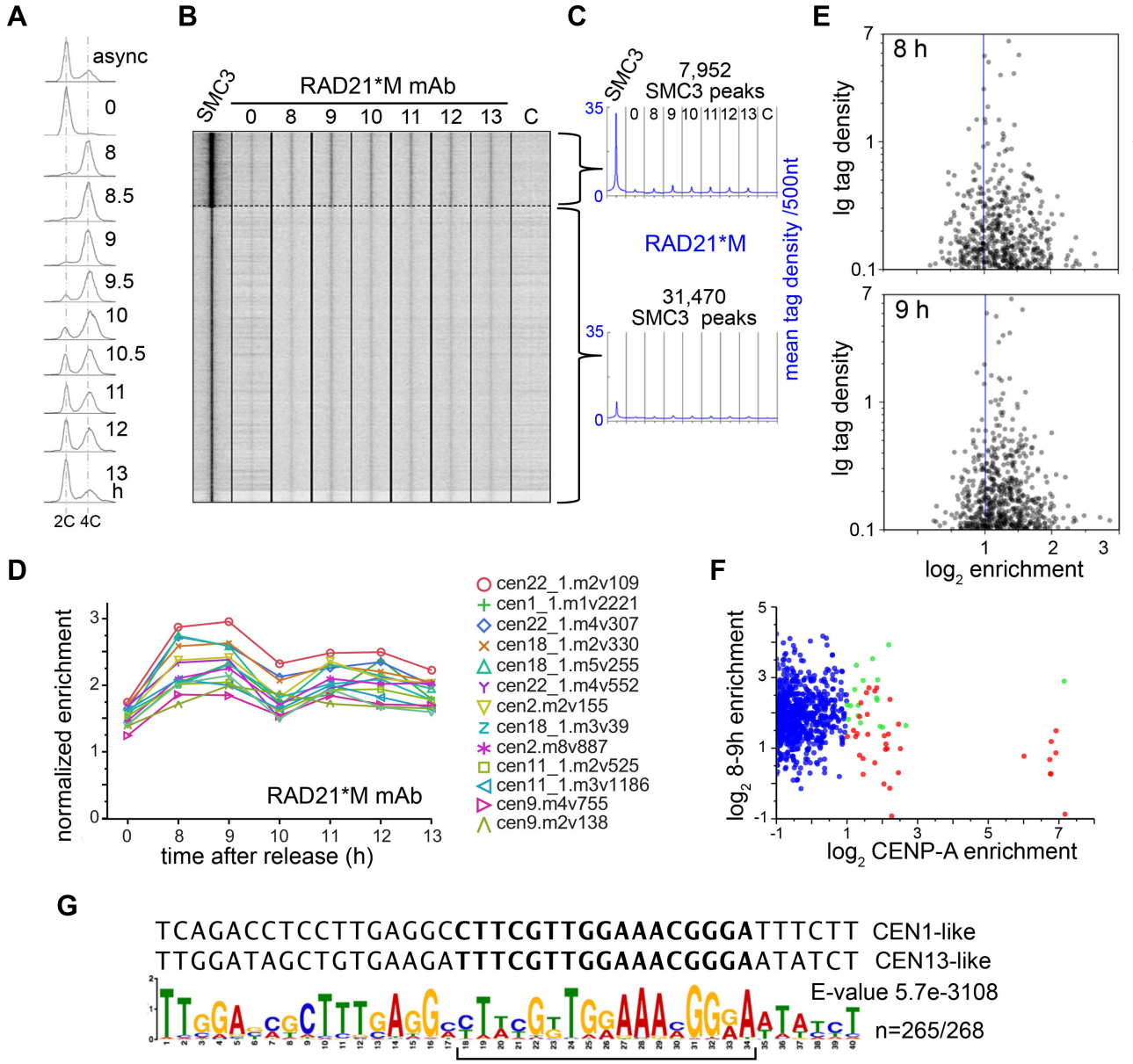

Figure 4. The validation of anti-RAD21* neo-epitope mAbs in metaphase-to-anaphase time course. (**A**) FACS of the DLD-1 cell population synchronized by double-thymidine block. After the release (time 0) the cells were collected at 30 min intervals starting with 8 h time point. These frequent sampling enabled to locate the transition from metaphase to anaphase with satisfactory precision between 8.5 h and 9.5 h. RAD21 was expected to be cleaved precisely at this time point, and specifically at centromeres. (**B**) Tag density heat map of sequence tags corresponding to strong and weak SMC3 peaks and the corresponding RAD21* neo-epitope tag density in the non-repeated part of the human genome during synchronous mitosis. The second site mAbs (1B22s and 2B16s, RAD21*M) binding, expressed and tag density, was normalized to the total number of aligned tags in the given data file. The peaks originating from extremely noisy regions were excluded by hierarchical clustering. Time points are as in (A). (**C**) The combined peak profiles of mean tag density from the datasets in (B). (**D**) The normalized fold enrichment over input for datasets in (B) versus centromeric alpha satellites showing the highest enrichment. Only ALRs with at least 500 hits (before normalization) in the IP are shown. Time points are as in (A). (**E**) A volcano plot of individual ALRs enrichment for RAD21* at 8 and 9 h. The graphs represent a 17,490 element subset of ALRs that satisfy the criteria of tag density ≥0.01 for both 8 and 9 h time-points. This subset overwhelmingly contains elements that have above zero enrichment. Additional filtering within this group for significantly enriched elements, i.e. tag density ≥ 0.1 and fold enrichment ≥ 2, gave 382 ALRs for 8 h and 463 for 9 h, with 269 ALRs in common. (**F**) A comparison of ALR enrichment for CENP-A and RAD21*. The plot shows relative enrichment for CENP-A and 8–9h average for RAD21* for a subset of 2,097 ALRs that had tag density ≥ 0.01 and fold enrichment ≥ 2 for either CENP-A, RAD21* 8 h, or RAD21* 9 h. 49 red points are enriched ≥ 2 for CENP-A but not RAD21* at either 8 h or 9 h, 18 green – enriched ≥2 for all of CENP-A, RAD21* 8 h, and RAD21* 9 h. 1200 points with $\log_2 <(-1)$ for CENP-A are cut off from the graph. (**G**) ALR consensus for repeats enriched at 8 and 9 h timepoints. The 269 ALRs enriched at both 8 and 9 h time points, as described in (E), were analyzed by MEME consensus algorithm. Two canonical HOR-forming ALRs are shown for comparison.

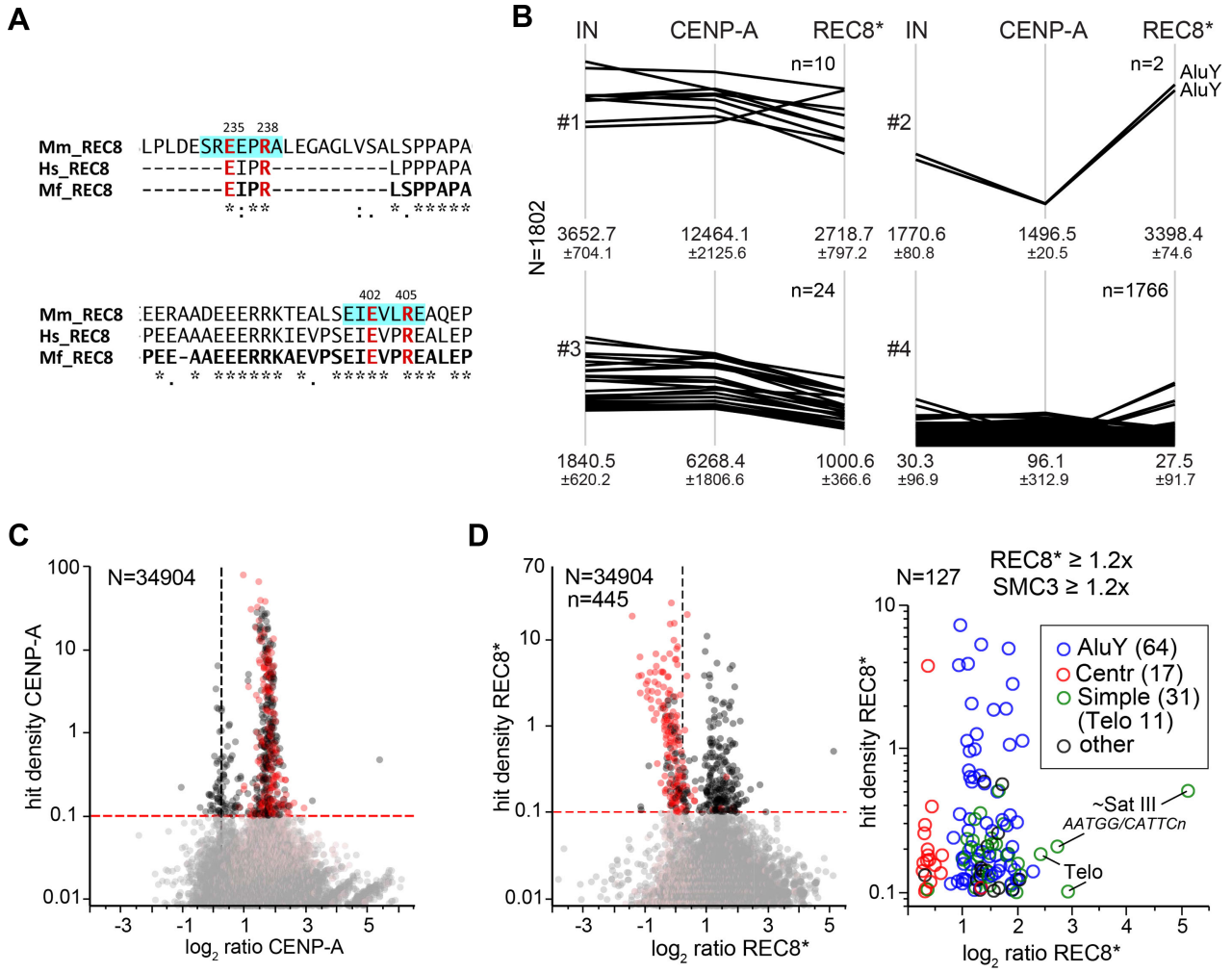

Figure 5. ChIP-on-ChEPseq analysis of repeats in macaque testis. (**A**) A comparison of mouse (Mm_REC8), human (Hs_REC8) and macaque (M_fREC8) REC8 regions harboring separase cleavage sites. The alignment was done using Mafft (mafft.cbrc.jp/alignment/software/) with BLOSUM 80 matrix. Shaded blue are confirmed primary cleavage sites in mouse REC8. The consensus residues of separase recognition sites are in bold red. (**B**) Parallel plots of hierarchical cluster analysis of CENP-A and REC8* enrichment at genomic repeats. Only repeats that had any enrichment for SMC3 and at least 10 normalized hits for any of input, CENP-A, or REC8* were included. Values shown below are normalized hits. (**C**) A volcano plot of normalized tag density at TR versus normalized enrichment for CENP-A. Red markers correspond to alpha-satellites. The total number of analyzed TR, i.e. with minimal length 120 nt, was 34 904, with 599 with tag density above 0.0083, i.e. one hit per a 120-nt sequence. The vertical dotted line corresponds to the cutoff at 1.2× enrichment. (**D**) The left chart shows a plot of normalized tag density at TR versus normalized enrichment over input for REC8*. Markers and cut-offs are as in (C). 445 elements had at least one hit per 120 nt. The right plot shows a subset of the same data, where both REC8* and SMC3 are enriched at least 1.2×. The marked sequences are examples of telomeric and centromeric TRs.

gions (CDRs), which are hyper-variable (82), with VH domains being the most diverse. As shown in Supplementary Figure S1B and C, the antibodies with close specificity have the most similar CDRs, suggesting a convergent pathway in generating the corresponding affinities.

Potential impact and applicability of separase cleavage mapping

The catalytic activity of separase is a key to both somatic cell proliferation and the gametogenesis (1,11), as well as to DNA damage repair (20–22). It is also well established that a disruption of separase function results in chromosome instability, which has been linked to diseases including cancers (83–85). In the particular case of gametogenesis, the critical importance of REC8 cleavage was initially demonstrated in yeast (11,86) and then confirmed for mouse spermatocytes (50). This REC8 proteolysis requirement in spermatogenesis appears to be multimodal: first for chiasmata resolution and chromosome segregation in meiosis I, and then, most likely, for chromatid segregation in meiosis II. Thus, REC8 cleavage is ultimately linked to the genetic homeostasis in human population, particularly in preventing chromosomal mutations common for cohesinopathies (87).

By developing a monoclonal antibody approach to specifically detect the neo-epitopes arising from the cleavage of REC8, combined with a proteomic approach to extract pure crosslinked chromatin, we were able to address the questions of cleavage preference for REC8 at centromeric repeats in a primate model. One of the limitations of our approach was that we did not detect any strong peaks specific for REC8* along chromosomal arms in testis, however

one might expect the location of cleavage to be dispersed along the binding sites for meiotic cohesin and to vary from one spermatocyte to another, due to the different position of chiasmata holding sites, as discussed in (70). Furthermore, the cleavage itself is believed to be confined to a small fraction of cells in the testis. At the same time, the preference for AluY could be meaningful, as these SINE repeats were shown, at least in one report (88), to coincide with SCE components in Macaque meiosis. Another technical limitation is, expectedly, the specificity of the mAbs. While the naturally occurring polypeptides terminating with sequences identical to our RAD21* and REC8* antigens apparently did not pose a problem, we cannot exclude a possibility of additional, yet unknown, substrates of separase being recognized. However, our adherence to analyzing only strongly chromatin-bound proteins and to using a positive control, i.e. the SMC3 subunit of cohesin complexes, likely alleviate that challenge.

Apart from the methodological implications of this work, we obtained some biologically relevant results, e.g. the demonstration that REC8 cleavage signal is distinct from the centromere core protein CENP-A, when centromeric repeats are interrogated for both signals, even within the subset of ALRs (62,71). While epigenomic analysis of highly homogeneous repeats is challenging, the utilization of CENP-A, which forms stable nucleosomes persisting through the cell cycle (77), as a relevant reference made our approach substantially more informative. Furthermore, we established that in somatic cells, RAD21 is likely cleaved in a similar positional fashion, with respect to CENP-A domains, possibly reflecting the modular structure of human kinetochores (73).

Finally, the inherent technical limitations in dealing with a complex organ containing only a miniscule fraction of cells in the desired state, i.e. undergoing REC8 cleavage, do not preclude a potential application of the method in the future, in order to pinpoint non-centromeric cleavage sites, which were predicted to exist. Particularly, these mAbs could be used, if/when epigenomic technologies adequately develop to facilitate single cell mapping of chromatin protein binding.

DATA AVAILABILITY

High-throughput sequencing data and the corresponding metadata are available from NCBI GEO with the accession numbers GSM5191858, GSM5191859, and GSE201989, for macaque, GSM4238560, GSM4238561 and GSM4238562 for human cells. mAbs cDNA sequences were deposited to GenBank with accession numbers OP292111-OP292120.

SUPPLEMENTARY DATA

Supplementary Data are available at NARGAB Online.

ACKNOWLEDGEMENTS

We thank former lab member C.C. Meng for the initial antibody testing; M. Tortotella (GIBH), Liu Wei (Huazhen Farm), Xiangyu Guo (Landao Co.) for macaque tissues; D. Loukinov for helpful advice on monoclonal antibody generation; and C. Ward for Tandem Repeat Finder analysis.

FUNDING

A.S. was supported by the MOST National Key R&D Program of China [2018YFA0106903]; Government of Guangdong province.
Conflict of interest statement. None declared.

REFERENCES

1. Uhlmann,F., Wernic,D., Poupart,M.A., Koonin,E.V. and Nasmyth,K. (2000) Cleavage of cohesin by the CD clan protease separin triggers anaphase in yeast. *Cell*, **103**, 375–386.
2. Viadiu,H., Stemmann,O., Kirschner,M.W. and Walz,T. (2005) Domain structure of separase and its binding to securin as determined by EM. *Nat. Struct. Mol. Biol.*, **12**, 552–553.
3. Lin,Z., Luo,X. and Yu,H. (2016) Structural basis of cohesin cleavage by separase. *Nature*, **532**, 131–134.
4. Boland,A., Martin,T.G., Zhang,Z., Yang,J., Bai,X.C., Chang,L., Scheres,S.H. and Barford,D. (2017) Cryo-EM structure of a metazoan separase-securin complex at near-atomic resolution. *Nat. Struct. Mol. Biol.*, **24**, 414–418.
5. Luo,S. and Tong,L. (2021) Structure and function of the separase-securin complex. *Subcell. Biochem.*, **96**, 217–232.
6. Sullivan,M., Lehane,C. and Uhlmann,F. (2001) Orchestrating anaphase and mitotic exit: separase cleavage and localization of Slk19. *Nat. Cell Biol.*, **3**, 771–777.
7. Sullivan,M. and Uhlmann,F. (2003) A non-proteolytic function of separase links the onset of anaphase to mitotic exit. *Nat. Cell Biol.*, **5**, 249–254.
8. Stegmeier,F., Visintin,R. and Amon,A. (2002) Separase, polo kinase, the kinetochore protein slk19, and spo12 function in a network that controls cdc14 localization during early anaphase. *Cell*, **108**, 207–220.
9. Queralt,E., Lehane,C., Novak,B. and Uhlmann,F. (2006) Downregulation of PP2A(Cdc55) phosphatase by separase initiates mitotic exit in budding yeast. *Cell*, **125**, 719–732.
10. Uhlmann,F., Lottspeich,F. and Nasmyth,K. (1999) Sister-chromatid separation at anaphase onset is promoted by cleavage of the cohesin subunit Scc1. *Nature*, **400**, 37–42.
11. Buonomo,S.B., Clyne,R.K., Fuchs,J., Loidl,J., Uhlmann,F. and Nasmyth,K. (2000) Disjunction of homologous chromosomes in meiosis I depends on proteolytic cleavage of the meiotic cohesin Rec8 by separin. *Cell*, **103**, 387–398.
12. Waizenegger,I.C., Hauf,S., Meinke,A. and Peters,J.M. (2000) Two distinct pathways remove mammalian cohesin from chromosome arms in prophase and from centromeres in anaphase. *Cell*, **103**, 399–410.
13. Hauf,S., Waizenegger,I.C. and Peters,J.M. (2001) Cohesin cleavage by separase required for anaphase and cytokinesis in human cells. *Science*, **293**, 1320–1323.
14. Baskerville,C., Segal,M. and Reed,S.I. (2008) The protease activity of yeast separase (esp1) is required for anaphase spindle elongation independently of its role in cleavage of cohesin. *Genetics*, **178**, 2361–2372.
15. Tsou,M.F., Wang,W.J., George,K.A., Uryu,K., Stearns,T. and Jallepalli,P.V. (2009) Polo kinase and separase regulate the mitotic licensing of centriole duplication in human cells. *Dev. Cell*, **17**, 344–354.
16. Nakamura,A., Arai,H. and Fujita,N. (2009) Centrosomal aki1 and cohesin function in separase-regulated centriole disengagement. *J. Cell Biol.*, **187**, 607–614.
17. Schockel,L., Mockel,M., Mayer,B., Boos,D. and Stemmann,O. (2011) Cleavage of cohesin rings coordinates the separation of centrioles and chromatids. *Nat. Cell Biol.*, **13**, 966–972.
18. Lee,K. and Rhee,K. (2012) Separase-dependent cleavage of pericentrin B is necessary and sufficient for centriole disengagement during mitosis. *Cell Cycle*, **11**, 2476–2485.
19. Matsuo,K., Ohsumi,K., Iwabuchi,M., Kawamata,T., Ono,Y. and Takahashi,M. (2012) Kendrin is a novel substrate for separase

involved in the licensing of centriole duplication. *Curr. Biol.*, **22**, 915–921.
20. Nagao,K., Adachi,Y. and Yanagida,M. (2004) Separase-mediated cleavage of cohesin at interphase is required for DNA repair. *Nature*, **430**, 1044–1048.
21. McAleenan,A., Clemente-Blanco,A., Cordon-Preciado,V., Sen,N., Esteras,M., Jarmuz,A. and Aragon,L. (2013) Post-replicative repair involves separase-dependent removal of the kleisin subunit of cohesin. *Nature*, **493**, 250–254.
22. Hellmuth,S., Gutierrez-Caballero,C., Llano,E., Pendas,A.M. and Stemmann,O. (2018) Local activation of mammalian separase in interphase promotes double-strand break repair and prevents oncogenic transformation. *EMBO J.*, **37**, e99184.
23. Baum,P., Yip,C., Goetsch,L. and Byers,B. (1988) A yeast gene essential for regulation of spindle pole duplication. *Mol. Cell. Biol.*, **8**, 5386–5397.
24. Uzawa,S., Samejima,I., Hirano,T., Tanaka,K. and Yanagida,M. (1990) The fission teast *cut1*$^{+}$ gene regulates spindle pole doby duplication and has homology to the budding yeast *ESP1* gene. *Cell*, **62**, 913–925.
25. May,G.S., McGoldrick,C.A., Holt,C.L. and Denison,S.H. (1992) The *bimB3* mutation of *Aspergillus nidulans* uncouples DNA replication from the completion of mitosis. *JBC*, **267**, 15737–15743.
26. Gorr,I.H., Boos,D. and Stemmann,O. (2005) Mutual inhibition of separase and cdk1 by two-step complex formation. *Mol. Cell*, **19**, 135–141.
27. Lianga,N., Dore,C., Kennedy,E.K., Yeh,E., Williams,E.C., Fortinez,C.M., Wang,A., Bloom,K.S. and Rudner,A.D. (2018) Cdk1 phosphorylation of esp1/separase functions with PP2A and slk19 to regulate pericentric cohesin and anaphase onset. *PLos Genet.*, **14**, e1007029.
28. Rosen,L.E., Klebba,J.E., Asfaha,J.B., Ghent,C.M., Campbell,M.G., Cheng,Y. and Morgan,D.O. (2019) Cohesin cleavage by separase is enhanced by a substrate motif distinct from the cleavage site. *Nat. Commun.*, **10**, 5189.
29. Hellmuth,S., Gomez,H.L., Pendas,A.M. and Stemmann,O. (2020) Securin-independent regulation of separase by checkpoint-induced shugoshin-MAD2. *Nature*, **580**, 536–541.
30. Yu,J., Raia,P., Ghent,C.M., Raisch,T., Sadian,Y., Cavadini,S., Sabale,P.M., Barford,D., Raunser,S., Morgan,D.O. *et al.* (2021) Structural basis of human separase regulation by securin and CDK1-cyclin B1. *Nature*, **596**, 138–142.
31. Zou,H., Stemman,O., Anderson,J.S., Mann,M. and Kirschner,M.W. (2002) Anaphase specific auto-cleavage of separase. *FEBS Lett.*, **528**, 246–250.
32. Monen,J., Hattersley,N., Muroyama,A., Stevens,D., Oegema,K. and Desai,A. (2015) Separase cleaves the N-Tail of the CENP-A related protein CPAR-1 at the meiosis i metaphase-anaphase transition in c. elegans. *PLoS One*, **10**, e0125382.
33. Weber,J., Kabakci,Z., Chaurasia,S., Brunner,E. and Lehner,C.F. (2020) Chromosome separation during drosophila male meiosis i requires separase-mediated cleavage of the homolog conjunction protein UNO. *PLoS Genet.*, **16**, e1008928.
34. Maier,N.K., Ma,J., Lampson,M.A. and Cheeseman,I.M. (2021) Separase cleaves the kinetochore protein meikin at the meiosis I/II transition. *Dev. Cell*, **56**, 2192–2206.
35. Bembenek,J.N., Richie,C.T., Squirrell,J.M., Campbell,J.M., Eliceiri,K.W., Poteryaev,D., Spang,A., Golden,A. and White,J.G. (2007) Cortical granule exocytosis in C. elegans is regulated by cell cycle components including separase. *Development*, **134**, 3837–3848.
36. Bai,X. and Bembenek,J.N. (2017) Protease dead separase inhibits chromosome segregation and RAB-11 vesicle trafficking. *Cell Cycle*, **16**, 1902–1917.
37. Bacac,M., Fusco,C., Planche,A., Santodomingo,J., Demaurex,N., Leemann-Zakaryan,R., Provero,P. and Stamenkovic,I. (2011) Securin and separase modulate membrane traffic by affecting endosomal acidification. *Traffic*, **12**, 615–626.
38. Bard,F., Casano,L., Mallabiabarrena,A., Wallace,E., Saito,K., Kitayama,H., Guizzunti,G., Hu,Y., Wendler,F., Dasgupta,R. *et al.* (2006) Functional genomics reveals genes involved in protein secretion and golgi organization. *Nature*, **439**, 604–607.
39. Vagnarelli,P., Morrison,C., Dodson,H., Sonoda,E., Takeda,S. and Earnshaw,W.C. (2004) Analysis of Scc1-deficient cells defines a key metaphase role of vertebrate cohesin in linking sister kinetochores. *EMBO Rep.*, **5**, 167–171.
40. Nakajima,M., Kumada,K., Hatakeyama,K., Noda,T., Peters,J.M. and Hirota,T. (2007) The complete removal of cohesin from chromosome arms depends on separase. *J. Cell Sci.*, **120**, 4188–4196.
41. Biswas,U., Hempel,K., Llano,E., Pendas,A. and Jessberger,R. (2016) Distinct roles of meiosis-specific cohesin complexes in mammalian spermatogenesis. *PLoS Genet.*, **12**, e1006389.
42. Lee,J. and Hirano,T. (2011) RAD21L, a novel cohesin subunit implicated in linking homologous chromosomes in mammalian meiosis. *J. Cell Biol.*, **192**, 263–276.
43. Ishiguro,K., Kim,J., Fujiyama-Nakamura,S., Kato,S. and Watanabe,Y. (2011) A new meiosis-specific cohesin complex implicated in the cohesin code for homologous pairing. *EMBO Rep.*, **12**, 267–275.
44. Herran,Y., Gutierrez-Caballero,C., Sanchez-Martin,M., Hernandez,T., Viera,A., Barbero,J.L., de Alava,E., de Rooij,D.G., Suja,J.A., Llano,E. *et al.* (2011) The cohesin subunit RAD21L functions in meiotic synapsis and exhibits sexual dimorphism in fertility. *EMBO J.*, **30**, 3091–3105.
45. Fukuda,T., Fukuda,N., Agostinho,A., Hernandez-Hernandez,A., Kouznetsova,A. and Hoog,C. (2014) STAG3-mediated stabilization of REC8 cohesin complexes promotes chromosome synapsis during meiosis. *EMBO J.*, **33**, 1243–1255.
46. Rong,M., Matsuda,A., Hiraoka,Y. and Lee,J. (2016) Meiotic cohesin subunits RAD21L and REC8 are positioned at distinct regions between lateral elements and transverse filaments in the synaptonemal complex of mouse spermatocytes. *J. Reprod. Dev.*, **62**, 623–630.
47. Agostinho,A., Manneberg,O., van Schendel,R., Hernandez-Hernandez,A., Kouznetsova,A., Blom,H., Brismar,H. and Hoog,C. (2016) High density of REC8 constrains sister chromatid axes and prevents illegitimate synaptonemal complex formation. *EMBO Rep.*, **17**, 901–913.
48. Ward,A., Hopkins,J., McKay,M., Murray,S. and Jordan,P.W. (2016) Genetic interactions between the meiosis-specific cohesin components, STAG3, REC8, and RAD21L. *G3*, **6**, 1713–1724.
49. Crawley,O., Barroso,C., Testori,S., Ferrandiz,N., Silva,N., Castellano-Pozo,M., Jaso-Tamame,A.L. and Martinez-Perez,E. (2016) Cohesin-interacting protein WAPL-1 regulates meiotic chromosome structure and cohesion by antagonizing specific cohesin complexes. *Elife*, **5**, e10851.
50. Kudo,N.R., Anger,M., Peters,A.H., Stemmann,O., Theussl,H.C., Helmhart,W., Kudo,H., Heyting,C. and Nasmyth,K. (2009) Role of cleavage by separase of the rec8 kleisin subunit of cohesin during mammalian meiosis I. *J. Cell Sci.*, **122**, 2686–2698.
51. Wysocka,J., Reilly,P.T. and Herr,W. (2001) Loss of HCF-1-chromatin association precedes temperature-induced growth arrest of tsBN67 cells. *Mol. Cell. Biol.*, **21**, 3820–3829.
52. Weatherall,D.J. (2006) In: *The use of non-human primates in research*. Working group report, p. 149.
53. Lankau,E.W., Turner,P.V., Mullan,R.J. and Galland,G.G. (2014) Use of nonhuman primates in research in North America. *J. Am. Assoc. Lab Anim. Sci.*, **53**, 278–282.
54. Kustatscher,G., Wills,K.L., Furlan,C. and Rappsilber,J. (2014) Chromatin enrichment for proteomics. *Nat. Protoc.*, **9**, 2090–2099.
55. Chen,S., Zhou,Y., Chen,Y. and Gu,J. (2018) fastp: an ultra-fast all-in-one FASTQ preprocessor. *Bioinformatics*, **34**, i884–i890.
56. Langmead,B., Trapnell,C., Pop,M. and Salzberg,S.L. (2009) Ultrafast and memory-efficient alignment of short DNA sequences to the human genome. *Genome Biol.*, **10**, R25.
57. Zhang,Y., Liu,T., Meyer,C.A., Eeckhoute,J., Johnson,D.S., Bernstein,B.E., Nusbaum,C., Myers,R.M., Brown,M., Li,W. *et al.* (2008) Model-based analysis of chip-Seq (MACS). *Genome Biol.*, **9**, R137.
58. Liu,T. (2014) Use model-based analysis of chip-Seq (MACS) to analyze short reads generated by sequencing protein-DNA interactions in embryonic stem cells. *Methods Mol. Biol.*, **1150**, 81–95.
59. Quinlan,A.R. (2014) BEDTools: the swiss-army tool for genome feature analysis. *Curr. Protoc. Bioinformatics*, **47**, 11-12-1–11-12.34.
60. Ramirez,F., Ryan,D.P., Gruning,B., Bhardwaj,V., Kilpert,F., Richter,A.S., Heyne,S., Dundar,F. and Manke,T. (2016) deepTools2: a next generation web server for deep-sequencing data analysis. *Nucleic Acids Res.*, **44**, W160–W165.

61. Ye,T., Krebs,A.R., Choukrallah,M.A., Keime,C., Plewniak,F., Davidson,I. and Tora,L. (2011) seqMINER: an integrated chip-seq data interpretation platform. *Nucleic Acids Res.*, **39**, e35.
62. Miga,K.H., Newton,Y., Jain,M., Altemose,N., Willard,H.F. and Kent,W.J. (2014) Centromere reference models for human chromosomes x and y satellite arrays. *Genome Res.*, **24**, 697–707.
63. Benson,G. (1999) Tandem repeats finder: a program to analyze DNA sequences. *Nucleic Acids Res.*, **27**, 573–580.
64. Gelfand,Y., Rodriguez,A. and Benson,G. (2007) TRDB–the tandem repeats database. *Nucleic Acids Res.*, **35**, D80–D87.
65. Waizenegger,I.C., Hauf,S., Meinke,A. and Peters,J.M. (2000) Two distinct pathways remove mammalian cohesin from chromosome arms in prophase and from centromeres in anaphase. *Cell*, **103**, 399–410.
66. Waizenegger,I., Gimenez-Abian,J.F., Wernic,D. and Peters,J.M. (2002) Regulation of human separase by securin binding and autocleavage. *Curr. Biol.*, **12**, 1368–1378.
67. Chestukhin,A., Pfeffer,C., Milligan,S., DeCaprio,J.A. and Pellman,D. (2003) Processing, localization, and requirement of human separase for normal anaphase progression. *Proc. Natl. Acad. Sci. U.S.A.*, **100**, 4574–4579.
68. Meyer,R., Fofanov,V., Panigrahi,A., Merchant,F., Zhang,N. and Pati,D. (2009) Overexpression and mislocalization of the chromosomal segregation protein separase in multiple human cancers. *Clin. Cancer Res.*, **15**, 2703–2710.
69. Landt,S.G., Marinov,G.K., Kundaje,A., Kheradpour,P., Pauli,F., Batzoglou,S., Bernstein,B.E., Bickel,P., Brown,J.B., Cayting,P. *et al.* (2012) ChIP-seq guidelines and practices of the ENCODE and modENCODE consortia. *Genome Res.*, **22**, 1813–1831.
70. Boukaba,A., Liu,J., Ward,C., Wu,Q., Arnaoutov,A., Liang,J., Pugacheva,E.M., Dasso,M., Lobanenkov,V., Esteban,M. *et al.* (2022) Ectopic expression of meiotic cohesin generates chromosome instability in cancer cell line. *Proc. Natl. Acad. Sci. U.S.A.*, **119**, e2204071119.
71. Hayden,K.E., Strome,E.D., Merrett,S.L., Lee,H.R., Rudd,M.K. and Willard,H.F. (2013) Sequences associated with centromere competency in the human genome. *Mol. Cell. Biol.*, **33**, 763–772.
72. Thakur,J. and Henikoff,S. (2016) CENPT bridges adjacent CENPA nucleosomes on young human alpha-satellite dimers. *Genome Res.*, **26**, 1178–1187.
73. Sacristan,C., Samejima,K., Ruiz,L.A., Lambers,M.L.A., Buckle,A., Brackley,C.A., Robertson,D., Hori,T., Webb,S., Fukagawa,T. *et al.* (2022) Condensin reorganizes centromeric chromatin during mitotic entry into a bipartite structure stabilized by cohesin. bioRxiv doi: https://doi.org/10.1101/2022.08.01.502248, 01 August 2022, preprint: not peer reviewed.
74. Nurk,S., Koren,S., Rhie,A., Rautiainen,M., Bzikadze,A.V., Mikheenko,A., Vollger,M.R., Altemose,N., Uralsky,L., Gershman,A. *et al.* (2022) The complete sequence of a human genome. *Science*, **376**, 44–53.
75. Altemose,N., Logsdon,G.A., Bzikadze,A.V., Sidhwani,P., Langley,S.A., Caldas,G.V., Hoyt,S.J., Uralsky,L., Ryabov,F.D., Shew,C.J. *et al.* (2022) Complete genomic and epigenetic maps of human centromeres. *Science*, **376**, eabl4178.
76. Earnshaw,W.C., Allshire,R.C., Black,B.E., Bloom,K., Brinkley,B.R., Brown,W., Cheeseman,I.M., Choo,K.H., Copenhaver,G.P., Deluca,J.G. *et al.* (2013) Esperanto for histones: CENP-A, not cenh3, is the centromeric histone H3 variant. *Chromosome Res.*, **21**, 101–106.
77. Nechemia-Arbely,Y., Fachinetti,D., Miga,K.H., Sekulic,N., Soni,G.V., Kim,D.H., Wong,A.K., Lee,A.Y., Nguyen,K., Dekker,C. *et al.* (2017) Human centromeric CENP-A chromatin is a homotypic, octameric nucleosome at all cell cycle points. *J. Cell Biol.*, **216**, 607–621.
78. Thakur,J. and Henikoff,S. (2018) Unexpected conformational variations of the human centromeric chromatin complex. *Genes Dev.*, **32**, 20–25.
79. Okamoto,Y., Nakano,M., Ohzeki,J., Larionov,V. and Masumoto,H. (2007) A minimal CENP-A core is required for nucleation and maintenance of a functional human centromere. *EMBO J.*, **26**, 1279–1291.
80. Cechova,M., Harris,R.S., Tomaszkiewicz,M., Arbeithuber,B., Chiaromonte,F. and Makova,K.D. (2019) High satellite repeat turnover in great apes studied with short- and long-read technologies. *Mol. Biol. Evol.*, **36**, 2415–2431.
81. Jarmuz,M., Glotzbach,C.D., Bailey,K.A., Bandyopadhyay,R. and Shaffer,L.G. (2007) The evolution of satellite III DNA subfamilies among primates. *Am. J. Hum. Genet.*, **80**, 495–501.
82. Schroeder,H.W. Jr and Cavacini,L. (2010) Structure and function of immunoglobulins. *J. Allergy Clin. Immunol.*, **125**, S41–S52.
83. Zhang,N., Ge,G., Meyer,R., Sethi,S., Basu,D., Pradhan,S., Zhao,Y.J., Li,X.N., Cai,W.W., El-Naggar,A.K. *et al.* (2008) Overexpression of separase induces aneuploidy and mammary tumorigenesis. *Proc. Natl. Acad. Sci. U.S.A.*, **105**, 13033–13038.
84. Mukherjee,M., Ge,G., Zhang,N., Huang,E., Nakamura,L.V., Minor,M., Fofanov,V., Rao,P.H., Herron,A. and Pati,D. (2011) Separase loss of function cooperates with the loss of p53 in the initiation and progression of T- and B-cell lymphoma, leukemia and aneuploidy in mice. *PLoS One*, **6**, e22167.
85. Mukherjee,M., Ge,G., Zhang,N., Edwards,D.G., Sumazin,P., Sharan,S.K., Rao,P.H., Medina,D. and Pati,D. (2014) MMTV-Espl1 transgenic mice develop aneuploid, estrogen receptor alpha (ERalpha)-positive mammary adenocarcinomas. *Oncogene*, **33**, 5511–5522.
86. Kitajima,T.S., Miyazaki,Y, Fau - Yamamoto,M., Yamamoto,M, Fau - Watanabe,Y. and Watanabe,Y. (2003) Rec8 cleavage by separase is required for meiotic nuclear divisions in fission. *EMBO J.*, **22**, 5643–5653.
87. Brooker,A.S. and Berkowitz,K.M. (2014) The roles of cohesins in mitosis, meiosis, and human health and disease. *Methods Mol. Biol.*, **1170**, 229–266.
88. Johnson,M.E., Rowsey,R.A., Shirley,S., Vandevoort,C., Bailey,J. and Hassold,T. (2013) A specific family of interspersed repeats (SINEs) facilitates meiotic synapsis in mammals. *Mol. Cytogenet.*, **6**, 1.